

Electronic Supplementary Information

Heterometal Expansion of Oxoziirconium Carboxylate Clusters

Jurii L. Malaestean, Manfred Speldrich, Arkady Ellern, Svetlana G. Baca and Paul Kögerler*

Experimental Section

Syntheses of complexes. The precursors $[\text{Mn}_3\text{O}(\text{ib})_6(\text{im})_3]\cdot 3\text{Hiz}$ (**6**), $[\text{Fe}_3\text{O}(\text{piv})_6(\text{H}_2\text{O})_3]\text{piv}\cdot 2\text{Hpiv}$ (**7**), $[\text{Zr}_6\text{O}_4(\text{OH})_4(\text{piv})_{12}]$ (**8**), and $[\text{Zr}_6\text{O}_4(\text{OH})_4(\text{ib})_{12}(\text{H}_2\text{O})]\cdot 3\text{Hib}$ (**9**) (im = imidazole) were prepared according to the previously reported procedures (see ref. 6, 7c, and S. W. Zhang, Y. G. Wie, Q. Liu, M. C. Shao and W. S. Zhou, *Polyhedron*, 1996, **15**, 1041; N. V. Gerbeleu, A. S. Batsanov, G. A. Timko, I. K. Struchkov, K. M. Indrichan, and G. A. Popovich, *Dokl. Akad. Nauk SSSR*, 1987, **293**, 364 (in Russian)).

[$\text{Fe}_2\text{Zr}_6\text{O}_6(\text{OH})_2(\text{piv})_{12}(\text{bdea})_2]$ ·MeCN·0.25 H₂O (1**).** N-butyldiethanolamine (0.085 ml, 0.51 mmol) was added to a mixture of **7** (0.09 g, 0.08 mmol) and **8** (0.1 g, 0.05 mmol) in 5 mL MeCN. The resulting solution was sealed in a PTFE-lined stainless steel reactor and heated to 120 °C for 10 h, then slowly cooled to room temperature over 48 h. Yellow crystals were collected by filtration, washed with MeCN and dried in air (yield: 0.05 g, 41.6% based on Zr). Elemental analysis, calculated (found) for $\text{C}_{88}\text{H}_{146}\text{Fe}_2\text{N}_2\text{O}_{36}\text{Zr}_6$ (without solvate molecules): C, 39.37 (38.98); H, 6.43 (6.34); N, 1.20 (1.31). IR data (KBr, cm⁻¹): 3414br/m, 2962m, 2927sh, 2868s, 1563s, 1484s, 1422s, 1360m, 1337m, 1229s, 1104m, 1031w, 906w, 786m.

[$\text{Mn}_2\text{Zr}_6\text{O}_6(\text{OH})_2(\text{ib})_{12}(\text{bdea})_2(\text{H}_2\text{O})_2$] (2**).** N-butyldiethanolamine (0.085 ml, 0.51 mmol) was added to a mixture of **6** (0.05 g, 0.04 mmol) and **9** (0.09 g, 0.04 mmol) in 5 mL MeCN. The resulting solution was stirred for 3 h, filtered off and left in a covered vial. Pink crystals formed within a few days, were collected by filtration, washed with MeCN and dried in air (yield: 0.06 g, 66.7% based on Zr). Elemental analysis, calculated (found) for $\text{C}_{64}\text{H}_{126}\text{Mn}_2\text{N}_2\text{O}_{38}\text{Zr}_6$: C, 35.19 (35.00); H, 5.91 (5.67); N, 1.28 (1.41). IR data (KBr, cm⁻¹): 3417br/m, 2967m, 2931sh, 2871w, 1573vs, 1473m, 1426s, 1359w, 1286w, 1260w, 1095m, 648m, 616m.

[$\text{Ni}_3\text{Zr}_6\text{O}_4(\text{OH})_4(\text{ib})_{12}(\text{bdea})_3]$ ·0.67MeCN (3**).** N-butyldiethanolamine (0.085 ml, 0.51 mmol) was added to a solution of **9** (0.09 g, 0.04 mmol) and $\text{Ni}(\text{NO}_3)_2\cdot 6\text{H}_2\text{O}$ (0.06 g, 0.2 mmol) in 5 mL MeCN. The resulting solution was refluxed for 1 h, filtered off and left in a covered vial. Green blue crystals were collected by filtration in a few days, washed with MeCN and dried in air (yield: 0.06 g, 54% based on Zr). Elemental analysis, calculated (found) for $\text{C}_{72}\text{H}_{145}\text{N}_3\text{Ni}_3\text{O}_{40}\text{Zr}_6$ (without solvate molecules): C, 36.40 (36.11); H, 6.15 (5.72); N, 1.77 (1.85). IR data (KBr, cm⁻¹): 3431br/m, 2963m, 2927sh, 2868w, 1621s, 1566s, 1478s, 1428s, 1358w, 1293w, 1228w, 1097m, 917m, 829w, 603w.

[$\text{Ni}_3\text{Zr}_6\text{O}_4(\text{OH})_4(\text{ib})_{10}(\text{PhO})_2(\text{bdea})_3]$ ·2MeCN (4**).** N-butyldiethanolamine (0.085 ml, 0.51 mmol) was added to a solution of **9** (0.09 g, 0.04 mmol), phenol (0.045 g, 0.47 mmol) and $\text{Ni}(\text{NO}_3)_2\cdot 6\text{H}_2\text{O}$ (0.06 g, 0.2 mmol) in 5 mL MeCN. The resulting solution was refluxed for 2 h, filtered off and left in a covered vial. Green blue crystals were collected by filtration in a few days, washed with MeCN and dried in air (yield: 0.05 g, 45.4% based on Zr). Elemental analysis, calculated (found) for $\text{C}_{76}\text{H}_{135}\text{N}_3\text{Ni}_3\text{O}_{36}\text{Zr}_6$ (without solvate molecules): C, 38.33 (38.12); H, 5.71 (5.59); N, 1.76 (1.81). IR data (KBr, cm⁻¹): 3435br/m, 2964m, 2929sh, 2870w, 1579vs, 1474s, 1426s, 1360w, 1294m, 1163m, 918m, 756m, 701w, 626m.

[$\text{Ni}_6\text{Zr}_6\text{O}_8(\text{ib})_{12}(\text{Hbdea})_6](\text{NO}_3)_2\cdot 4\text{PhOH}$ (5**).** N-butyldiethanolamine (0.085 ml, 0.51 mmol) was added to a solution of **9** (0.09 g, 0.04 mmol), phenol (0.09 g, 0.95 mmol) and $\text{Ni}(\text{NO}_3)_2\cdot 6\text{H}_2\text{O}$ (0.06 g, 0.2 mmol)

in 5 mL MeCN. The resulting solution was refluxed for 5 h, filtered off and left in a covered vial. Green crystals were collected by filtration, washed with MeCN and dried in air (yield: 0.06 g, 40% based on Zr). Elemental analysis, calculated (found) for C₉₆H₁₆₈N₅Ni₆O₄₈Zr₆: C, 40.83 (40.57); H, 6.34 (6.00); N, 3.17 (3.15). IR data (KBr, cm⁻¹): 3223br/m, 2961m, 2871m, 1622vs, 1472s, 1427s, 1376m, 1293m, 1102m, 1016, 910m, 841w, 754m, 693m, 624m, 484m.

Magnetochemical Analysis

The computational framework CONDON is used for the analysis of the magnetic susceptibility data of compounds **1–5**. CONDON allows the simulation of both intramolecular exchange coupling and single-ion effects: interelectronic repulsion (H_{ee}), spin-orbit coupling (H_{so}), ligand-field effect (H_{lf}), and the Zeeman effect of an applied field (H_{mag}).¹

Theoretical modeling: The spin Hamiltonian of a single d^N metal ion in a ligand field environment of a distinct point symmetry in a static magnetic field \mathbf{B} is represented by

$$\hat{H} = \underbrace{\sum_{i=1}^N \left[-\frac{\hbar}{2m_e} \nabla_i^2 + V(r_i) \right]}_{\hat{H}^{(0)}} + \underbrace{\sum_{i>j} \frac{e^2}{r_{ij}}}_{\hat{H}_{ee}} + \underbrace{\sum_{i=1}^N \zeta(r_i) \kappa \hat{l}_i \cdot \hat{s}_i}_{\hat{H}_{so}} + \underbrace{\sum_{i=1}^N \sum_{k=0}^{\infty} \left\{ B_0^k C_0^k(i) + \sum_{q=2}^k [B_q^k (C_{-q}^k(i) + (-1)^q C_q^k(i))] \right\}}_{\hat{H}_{lf}} + \underbrace{\sum_{i=1}^N \mu_B (\kappa \hat{l}_i + 2 \hat{s}_i) \cdot \mathbf{B}}_{\hat{H}_{mag}}$$

where $H^{(0)}$ represents the energy in the central field approximation, H_{ee} and H_{so} account for interelectronic repulsion and spin-orbit coupling (modified by the orbital reduction factor κ), respectively. The former is taken into account by the Slater-Condon parameters F^2, F^4, F^6 , the latter by the one-electron spin-orbit coupling parameter ζ . These sets of interelectronic repulsion parameters as well as ζ and κ are used as constants in the fitting calculations.

H_{lf} represents the electrostatic effect of the ligands in the framework of ligand field theory on the basis of the global parameters B_q^k . The spherical tensors C_q^k are directly related to the spherical harmonics $C_q^k = \sqrt{4\pi(2k+1)} Y_q^k$ and the real ligand field parameters B_q^k (Wybourne notation) are given by $A_q^k \langle r^k \rangle$ where A_q^k is a numerical constant describing the charge distribution in the environment of the metal ion and $\langle r^k \rangle$ is the expectation value of $\langle r^k \rangle$ for the wave function.

For d electrons the terms in the expansion with $k \leq 4$ are nonzero, whereas all terms with odd k values vanish since we consider only configurations containing equivalent electrons. The values of k and q are limited by the point symmetry of the metal ion site. If the spherically symmetric term $B_0^0 C_0^0$ (which does not cause any splitting) is ignored, in cubic systems only spherical tensors with $k = 4$ are relevant and all B_q^k are zero. The ligand field operator with reference to the C_4 axis for the angular part of the wave function reads

$$H_{lf}^{\text{cub}} = B_0^4 \sum_{i=1}^N C_0^4(i) + \sqrt{5/14} (C_4^4(i) + C_{-4}^4(i))$$

Here, a fixed relation $B_4^4 = \sqrt{5/14} B_0^4$ exist, so that only the coefficient B_0^4 is essential; N is the number of electrons.

Exchange interactions between the spin centers are described by a Heisenberg-Dirac-Vleck operator of the type

$$\hat{H}_{\text{ex}} = -J\hat{\mathbf{S}}_1 \cdot \hat{\mathbf{S}}_2$$

In the high-temperature limit the Weiss temperature θ contains the contributions of all interactions between magnetic centers according to

$$\theta = \frac{2S(S+1)}{3k_B} \sum_i z_i J_i$$

where z_i is the number of neighbors with the interaction characterized by the coupling constant J_i (with $i = 1$ indicating nearest-neighbor interactions, $i = 2$ next-nearest neighbor interactions, etc.)

The values for spin-orbit coupling constants ζ and Racah parameters were determined from optical spectra, respectively and used as constant during the calculations (see Table S1).

Table S1: Magnetochemical parameters

Compound	1	2	3	4	5
Magnetic centers	Fe ³⁺ (3d ⁵)	Mn ³⁺ (3d ⁴)		Ni ²⁺ (3d ⁸)	
$B, C / \text{cm}^{-1}$	1058, 3900	990, 3680		1080, 4860	
ζ / cm^{-1}	400	270		600	
θ / K	-0.5	-0.4	-4.6	-2.3	-9.8
$C / \text{cm}^3 \text{K mol}^{-1}$	4.380	2.981	1.259	1.266	1.193
$B_{0:}^4$	-	19900	21100	21100	26000
g_{iso}	1.999	1.994	2.22	2.22	2.19
J / cm^{-1}	-0.14	-0.12	-2.4	-1.2	-4.12 (J_1) -1.56 (J_2)
SQ	0.9%	0.9%	0.8%	0.8%	1.0%
$\chi_{\text{dia}} / 10^{-3} \text{ cm}^3 \text{mol}^{-1}$	-1.183	-1.093	-3.609	-1.237	-1.767

$$SQ = \sqrt{\sum_{i=1}^n ([\chi_{\text{obs}}(i) - \chi_{\text{cal}}(i)] / \chi_{\text{obs}}(i))^2}$$

Compounds **1** and **2**

Due to its electronic configuration (3d⁵) and the resulting singlet term ⁶S_{5/2} of the free Fe³⁺ ion, the {Fe₂Zr₆} cluster in **1** should represent a pure spin Curie paramagnet in the absence of exchange interactions and saturation effects. Above 50 K, the low-field (0.1 Tesla) susceptibility is reproduced by a Curie-Weiss expression, $\chi_m = C/(T - \theta)$ with $C = 4.380 \text{ cm}^3 \text{K mol}^{-1}$ and $\theta = -0.5 \text{ K}$. The experimentally determined effective Bohr magneton number (μ_{eff}) approaches a value of 5.92 μ_B per magnetic center towards 300 K, exactly matching that of an $s = 5/2$ ($g = 2.0$) system. At 2.0 K, the field dependence of the molar susceptibility follows the corresponding Brillouin expression.

The Mn³⁺ ion exhibits a ⁵D₀ ground state with $S = 2$ in octahedral high-spin environments. Due to its electronic configuration (3d⁴) and the resulting doublet term ⁵E of the Mn³⁺ ion, the cluster in **2** should

exhibit Curie behavior if the ligand field strength Dq^1 is in the range from 500 cm^{-1} up to 1500 cm^{-1} , again as long as exchange interactions and saturation effects play no significant role. At room temperature the effective Bohr magneton number per Mn^{3+} ion is 4.9. The χ_m^{-1} vs. T plot shows a linear range between 80 and 290 K. This observation is supported by a linear fit reciprocal molar susceptibility to the Curie law above 30 K, leading to $C = 2.981\text{ cm}^3\text{ K mol}^{-1}$ and a Weiss constant $\theta = -0.4\text{ K}$. We note that the experimentally derived magnetic moment from the Curie constant C is equal to 4.87 and is very close to the pure spin system (Mn^{3+} , ligand field ground state 5E , four unpaired electrons, $S = 2$, $\mu_{\text{so}} = g\sqrt{S(S+1)} = 4.92\text{ }\mu_{\text{B}}$ with $g \approx 2$).

Compounds 3 and 4

The $3d^8$ systems **3** and **4** (free ion ground term 3F_4) show a nearly temperature independent effective Bohr magneton number of 3.15 down to ca. 100 K. The χ_m^{-1} vs. T plot shows Curie-Weiss-type behavior between 40 and 290 K, leading to $C = 1.259$ (**3**) and $C = 1.266\text{ cm}^3\text{ K mol}^{-1}$ (**4**) with $\theta = -4.6$ and -2.3 K . Excellent agreement between the experimental data and data simulated with CONDON was achieved when a uniform Heisenberg-type exchange interaction is used:

$$\hat{H}_{\text{ex}} = -J[\hat{\mathbf{S}}_1 \cdot \hat{\mathbf{S}}_2 + \hat{\mathbf{S}}_2 \cdot \hat{\mathbf{S}}_3 + \hat{\mathbf{S}}_1 \cdot \hat{\mathbf{S}}_3]$$

The derived values for J correspond to $\theta = -4.6\text{ K}$ and $\theta = -2.3\text{ K}$ for a pure spin system, along with contributions of the ligand field, interelectronic repulsion, spin-orbit coupling and external magnetic field. The calculated ligand field parameter $B_0^4 = 21100\text{ cm}^{-1}$ corresponds to a g_{iso} value of 2.22 for a pure spin system that takes into account ligand field effects.

Compound 5

The molar susceptibility (Fig. 3, inset) of compound **5** displays a sharp maximum at 5.0 K characteristic of antiferromagnetic exchange coupling. The susceptibility data can be described by a Curie-Weiss-type expression above 80 K, leading to $C = 1.193\text{ cm}^3\text{ K mol}^{-1}$ and a Weiss constant $\theta = -9.8\text{ K}$. The intramolecular exchange interactions between the six Ni^{II} centers are described using a spin Hamiltonian augmented by a Heisenberg-type exchange operator that differentiates two exchange pathways:

$$\hat{H}_{\text{ex}} = -J_1[\hat{\mathbf{S}}_1 \cdot \hat{\mathbf{S}}_6 + \hat{\mathbf{S}}_2 \cdot \hat{\mathbf{S}}_3 + \hat{\mathbf{S}}_4 \cdot \hat{\mathbf{S}}_5] - J_2[\hat{\mathbf{S}}_1 \cdot \hat{\mathbf{S}}_2 + \hat{\mathbf{S}}_1 \cdot \hat{\mathbf{S}}_3 + \hat{\mathbf{S}}_2 \cdot \hat{\mathbf{S}}_4 + \hat{\mathbf{S}}_2 \cdot \hat{\mathbf{S}}_5 + \hat{\mathbf{S}}_3 \cdot \hat{\mathbf{S}}_4 + \hat{\mathbf{S}}_3 \cdot \hat{\mathbf{S}}_6 + \hat{\mathbf{S}}_4 \cdot \hat{\mathbf{S}}_6 + \hat{\mathbf{S}}_5 \cdot \hat{\mathbf{S}}_6]$$

An excellent agreement to the experimental data is found for $J_1 = -2.06\text{ cm}^{-1}$ and $J_2 = -1.52\text{ cm}^{-1}$ which corresponds to a Weiss temperature of $\theta = -9.8\text{ K}$. The calculated g_{iso} value of 2.19 corresponds to the ligand field parameter $B_0^4 = 26000\text{ cm}^{-1}$.

¹ Note the fixed relation in octahedral systems between Dq and ligand field parameter B_0^4 in Wybourne notation: $B_0^4 = 21Dq$

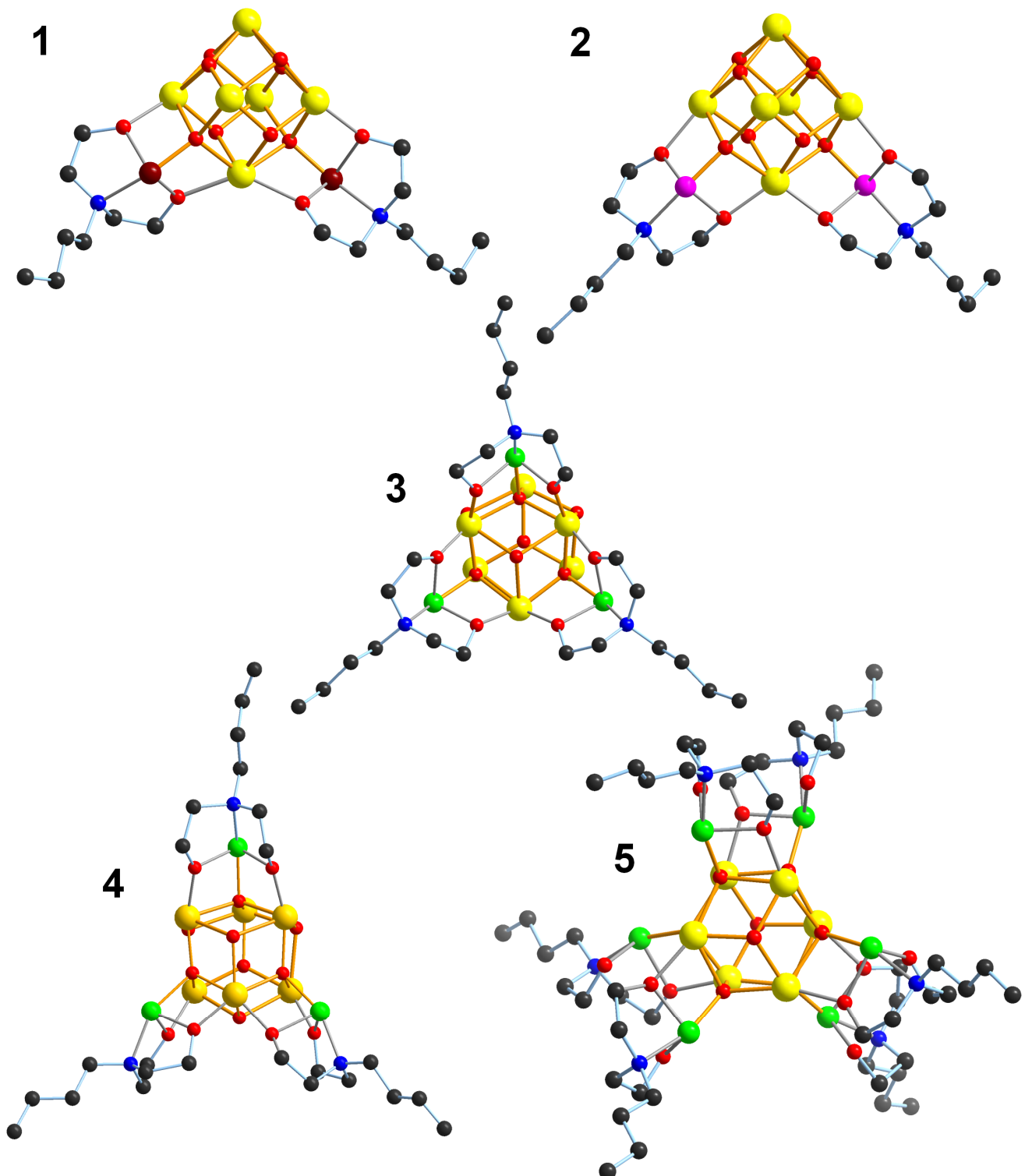


Figure S1. Structures of the $\{\text{Zr}_6(\text{Mbdea})_n\}$ subfragments illustrating the $\kappa N, \kappa^2 O, O'$ binding modes of the bdea^{2-} (**1–4**) and bdeah^- (**5**) ligands to the $\text{M}^{\text{II}/\text{III}}$ centers. Note that in **1–4**, the bdea^{2-} groups also coordinate to two adjacent Zr^{IV} sites whereas the monoprotonated bdeah^- groups in **5** bind to the $\{\text{Zr}_6\text{O}_8\}$ core only via one alkoxide O site. Color codes as in Fig. 2.

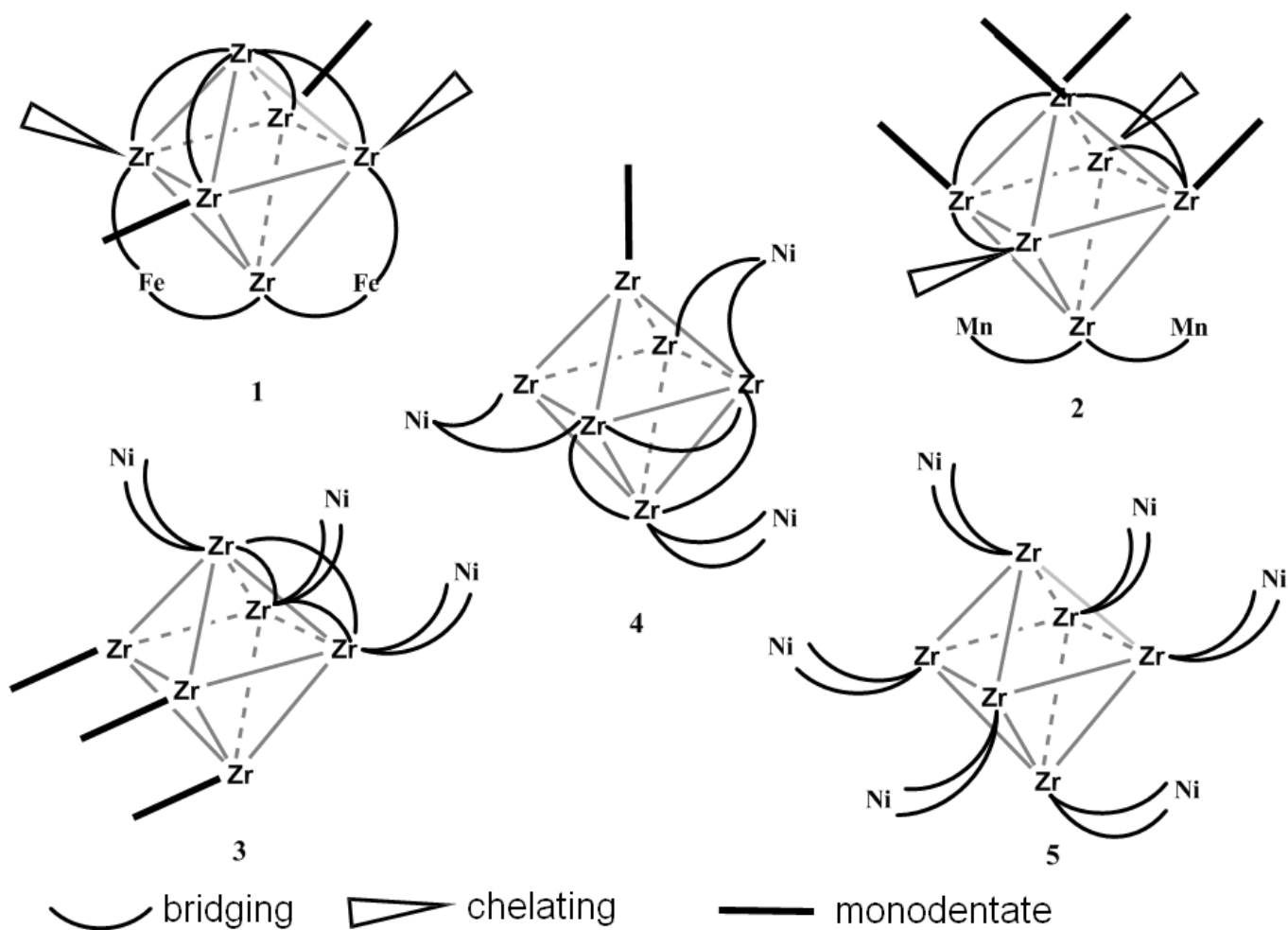


Figure S2. Schematic representation of coordination modes of carboxylate ligands in **1–5** (pivalates in **1** and isobutyrates in **2–5**). In **1** eight pivalates form bridges between both Zr atoms and Zr and Fe atoms, coordinating to the metal sites in the usual μ_2 -1,3 coordination fashion: four of them stabilize the $\{\text{Zr}_6\text{O}_4(\text{OH})_4\}^{12+}$ core bridging Zr···Zr edges and the other four pivalates connect two Fe sites to the oxozirconium cluster. Three other pivalate ligands function as chelate ligands whereas the remaining two pivalate ligands are coordinated to Zr atoms in a monodentate fashion. In **2** only six isobutyrate ligands form bidentate bridges: four carboxylates link Zr···Zr edges in the octahedron as in **1**, and two Mn atoms are bridged to the oxozirconium cluster by only two isobutyrate groups; two other carboxylate moieties are chelating and finally four isobutyrates are monodentate ligands coordinated to Zr atoms. In **3** the isobutyrate ligands display two types of coordination modes, bridging and monodentate: nine carboxylate moieties act as bridging ligands, three of them bridge Zr atoms in the octahedron, three other carboxylates link the three nickel atoms to the zirconium atoms of the Zr₆ polyhedron, each of the remaining three isobutyrate ligands is coordinating to the zirconium atoms in a monodentate mode. Out of the ten isobutyrate in compound **4** only one carboxylate is bound in a monodentate fashion to a Zr atom, whereas six other isobutyrate ligands are bridging the Ni atoms to the Zr₆ octahedron and the remaining three isobutyrate bridged the edges of the Zr₆ octahedron. In complex **5** all twelve carboxylate ligands behave as bridging one and each of six Ni atoms connected to the oxozirconium Zr₆O₈ core by two carboxylate bridging groups.

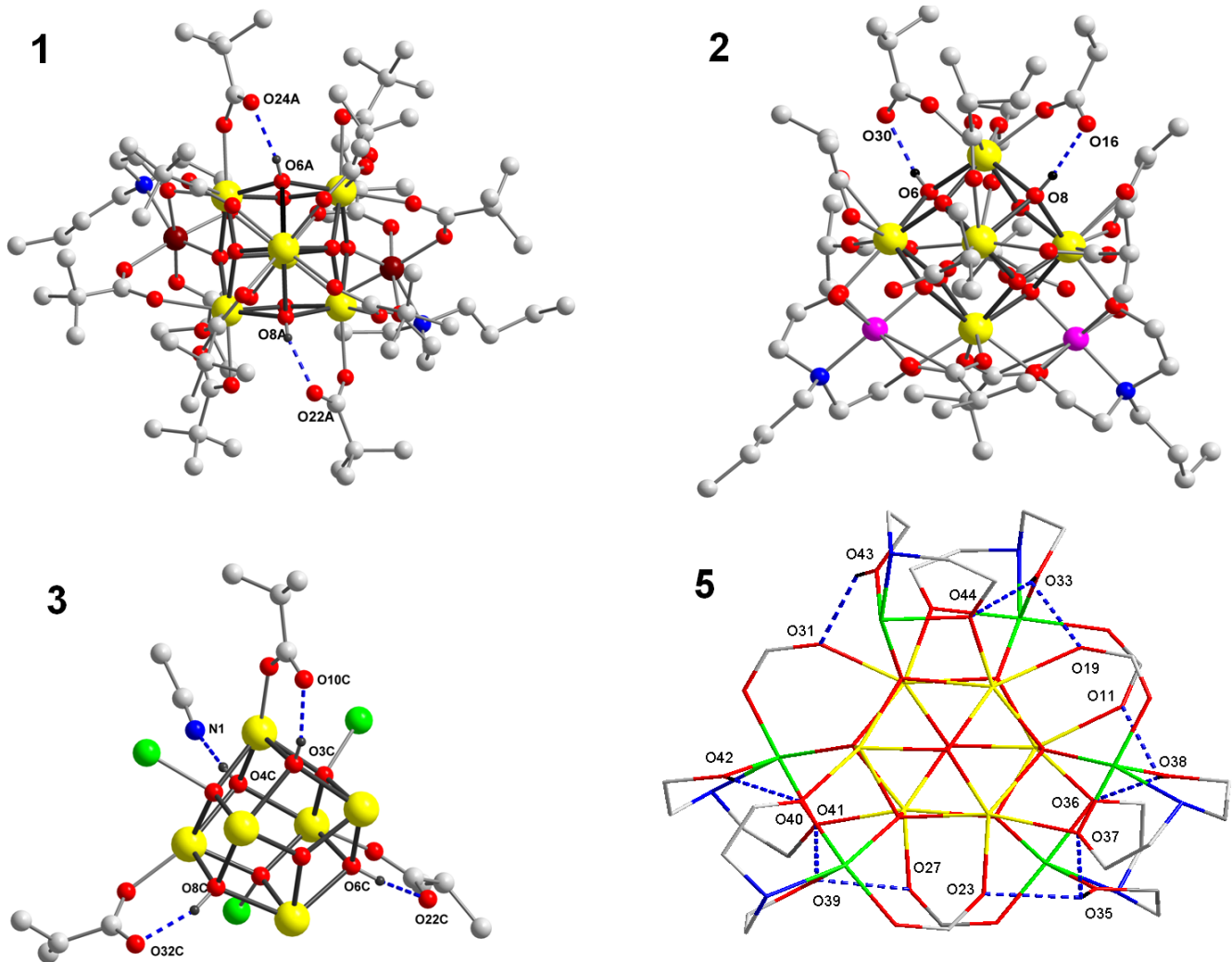


Figure S3. Intramolecular hydrogen bonds (dashed blue lines) in **1**, **2**, **3**, and **5**.

Table S1. Bond valence sum calculations for Fe, Mn and Ni sites in compounds **1–5**

		Assignment
Compound 1		
Fe1A	3.167	Fe ³⁺
Fe2A	3.217	Fe ³⁺
Fe1B	3.186	Fe ³⁺
Fe2B	3.170	Fe ³⁺
Compound 2		
Mn1	3.126	Mn ³⁺
Mn2	3.166	Mn ³⁺
Compound 3		
Ni1A	2.163	Ni ²⁺
Ni2A	2.111	Ni ²⁺
Ni3A	2.164	Ni ²⁺
Ni1B	2.119	Ni ²⁺
Ni2B	2.148	Ni ²⁺
Ni3B	2.194	Ni ²⁺
Ni1C	2.128	Ni ²⁺
Ni2C	2.156	Ni ²⁺
Ni3C	2.101	Ni ²⁺
Compound 4		
Ni1	2.096	Ni ²⁺
Ni2	2.076	Ni ²⁺
Ni3	2.120	Ni ²⁺
Compound 5		
Ni1	2.073	Ni ²⁺
Ni2	2.065	Ni ²⁺
Ni3	2.109	Ni ²⁺
Ni4	2.044	Ni ²⁺
Ni5	2.085	Ni ²⁺
Ni6	2.058	Ni ²⁺

Table S2. Selected bond distances (\AA) between Zr ions and $\mu_3\text{-O(H)}$ in $\{\text{Zr}_6\text{O}_8\}$ in **1-4**

1 $\{\text{Fe}_2\text{Zr}_6\}$					
Zr(2A)-O(6A)	2.364(4)	Zr(2A)-O(8A)	2.347(4)		
Zr(5A)-O(6A)	2.175(4)	Zr(3A)-O(8A)	2.159(4)		
Zr(6A)-O(6A)	2.221(4)	Zr(4A)-O(8A)	2.218(4)		
Zr(2B)-O(6B)	2.369(4)	Zr(2B)-O(8B)	2.375(4)		
Zr(5B)-O(6B)	2.186(4)	Zr(3B)-O(8B)	2.171(4)		
Zr(6B)-O(6B)	2.221(4)	Zr(4B)-O(8B)	2.225(4)		
2 $\{\text{Mn}_2\text{Zr}_6\}$					
Zr(2)-O(6)	2.306(6)	Zr(2)-O(8)	2.305(6)		
Zr(5)-O(6)	2.235(7)	Zr(3)-O(8)	2.222(6)		
Zr(6)-O(6)	2.269(6)	Zr(4)-O(8)	2.274(7)		
3 $\{\text{Ni}_3\text{Zr}_6\}$					
Zr(1A)-O(3A)	2.166(4)	Zr(1B)-O(3B)	2.164(4)	Zr(1C)-O(3C)	2.181(4)
Zr(5A)-O(3A)	2.329(4)	Zr(5B)-O(3B)	2.320(4)	Zr(5C)-O(3C)	2.302(4)
Zr(6A)-O(3A)	2.321(3)	Zr(6B)-O(3B)	2.318(4)	Zr(6C)-O(3C)	2.314(4)
Zr(1A)-O(4A)	2.312(4)	Zr(1B)-O(4B)	2.312(4)	Zr(1C)-O(4C)	2.314(4)
Zr(3A)-O(4A)	2.328(4)	Zr(3B)-O(4B)	2.318(4)	Zr(3C)-O(4C)	2.292(4)
Zr(4A)-O(4A)	2.332(4)	Zr(4B)-O(4B)	2.329(4)	Zr(4C)-O(4C)	2.300(4)
Zr(2A)-O(6A)	2.340(4)	Zr(2B)-O(6B)	2.336(4)	Zr(2C)-O(8C)	2.312(4)
Zr(4A)-O(6A)	2.154(4)	Zr(4B)-O(6B)	2.156(4)	Zr(4C)-O(6C)	2.167(4)
Zr(5A)-O(6A)	2.333(4)	Zr(5B)-O(6B)	2.329(4)	Zr(5C)-O(6C)	2.323(4)
Zr(2A)-O(8A)	2.316(4)	Zr(2B)-O(8B)	2.323(4)	Zr(2C)-O(6C)	2.311(4)
Zr(3A)-O(8A)	2.171(4)	Zr(3B)-O(8B)	2.170(4)	Zr(3C)-O(8C)	2.179(4)
Zr(6A)-O(8A)	2.305(4)	Zr(6B)-O(8B)	2.302(4)	Zr(6C)-O(8C)	2.301(4)
4 $\{\text{Ni}_3\text{Zr}_6\}$					
Zr(1)-O(2)	2.189(2)	Zr(4)-O(7)	2.207(2)		
Zr(4)-O(2)	2.298(2)	Zr(5)-O(8)	2.219(2)		
Zr(5)-O(2)	2.298(2)	Zr(6)-O(8)	2.331(2)		
Zr(3)-O(4)	2.344(2)	Zr(2)-O(8)	2.285(2)		
Zr(6)-O(4)	2.349(2)				
Zr(1)-O(4)	2.218(2)				
Zr(3)-O(7)	2.317(2)				
Zr(2)-O(7)	2.312(2)				

Table S3. Crystal data and details of crystallographic refinements

Empirical formula	1	2	3	4	5
Formula weight (g mol ⁻¹)	C ₇₈ H _{147.5} Fe ₂ N ₃ O _{36.25} Zr ₆	C ₆₄ H ₁₂₄ Mn ₂ N ₂ O ₃₈ Zr ₆	C ₂₂₀ H ₄₂₅ N ₁₁ Ni ₉ O ₁₄ Zr ₁₈	C ₈₀ H ₁₄₁ N ₅ Ni ₃ O ₃₆ Zr ₆	C ₁₂₀ H ₂₁₆₅ N ₈ Ni ₆ O ₅₄ Zr ₆
Temperature (K)	2366.51 130(2)	2186.85 173(2)	7219.06 153(2)	2472.43 130(2)	3534.59 143(2)
Wavelength (Å)	0.71073	0.71073	0.71073	0.71073	0.71073
Crystal system	Monoclinic	Orthorhombic	Triclinic	Triclinic	Triclinic
Space group	P _n	P2(1)2(1)2(1)	P- <i>I</i>	P- <i>I</i>	P- <i>I</i>
<i>a</i> (Å)	16.2199(8)	14.350(1)	14.945(3)	15.269(7)	15.269(7)
<i>b</i> (Å)	24.6037(1)	16.034(2)	20.363(7)	17.907(8)	17.907(8)
<i>c</i> (Å)	26.3241(1)	23.32(2)	31.919(1)	15.548(3)	28.743(1)
α (°)	90	102.439(2)	47.502(2)	25.356(5)	83.343(1)
β (°)	90.2200(1)	95.803(2)	90	77.22(3)	75.143(1)
γ (°)	90	115.106(2)	90	75.05(3)	76.450(1)
V (Å ³)	10505.1(9)	4631(9)	30874.2(2)	5113.0(17)	7371.9(6)
<i>Z</i>	4	2	4	2	2
<i>D_c</i> (g cm ⁻³)	1.496	1.568	1.553	1.606	1.592
μ (mm ⁻¹)	0.915	0.991	1.196	1.205	1.239
F(000)	4872	2232	14816	2535	3664
θ range for data collection (°)	2.16 to 22.30	1.67 to 21.97	0.77 to 26.43	0.84 to 30.83	1.42 to 25.00
Index ranges	-19 ≤ <i>h</i> ≤ 19, -29 ≤ <i>k</i> ≤ 29, -31 ≤ <i>l</i> ≤ 31	-15 ≤ <i>h</i> ≤ 15, -16 ≤ <i>k</i> ≤ 16, -24 ≤ <i>l</i> ≤ 24	-25 ≤ <i>h</i> ≤ 25, -39 ≤ <i>k</i> ≤ 39, -59 ≤ <i>l</i> ≤ 59	-21 ≤ <i>h</i> ≤ 21, -21 ≤ <i>k</i> ≤ 21, -35 ≤ <i>l</i> ≤ 35	-18 ≤ <i>h</i> ≤ 18, -21 ≤ <i>k</i> ≤ 21, -34 ≤ <i>l</i> ≤ 34
Reflections collected	111847	26640	277215	77385	58657
Reflections unique	36869	11275	63297	29359	25822
[R(int) = 0.0667]	[R(int) = 0.0822]	[R(int) = 0.0753]	[R(int) = 0.0459]	[R(int) = 0.0313]	[R(int) = 0.0313]
Completeness to θ_{max}	99.9%	99.7%	99.8%	91.3%	99.4%
Data / restraints / parameters	36869 / 126 / 2285	11275 / 90 / 1010	63297 / 93 / 3365	29359 / 273 / 1193	25822 / 0 / 1748
Final R indices [<i>I</i> > 2σ(<i>I</i>)]	R1 = 0.0387, wR2 = 0.0683	R1 = 0.0574, wR2 = 0.1270	R1 = 0.0596, wR2 = 0.1357	R1 = 0.0467, wR2 = 0.1296	R1 = 0.0363, wR2 = 0.0903
R indices (all data)	R1 = 0.0547, wR2 = 0.0710	R1 = 0.1149, wR2 = 0.1519	R1 = 0.0911, wR2 = 0.1528	R1 = 0.0651, wR2 = 0.1429	R1 = 0.0529, wR2 = 0.1049

Goodness-of-fit on F^2 | 0.827 | 1.045 | 1.087 | 1.038 | 1.040
